

Evolution of the spiral structure of galaxies from the HST COSMOS field

V.P. Reshetnikov^{1,2}, A.A. Marchuk^{1,2}, I.V. Chugunov^{1,2},
P.A. Usachev^{1,2}, and A.V. Mosenkov^{3,2}

¹ St.Petersburg State University, Universitetskii pr. 28, St.Petersburg, 198504 Russia

² Pulkovo Astronomical Observatory, Russian Academy of Sciences, St. Petersburg, 196140 Russia

³ Brigham Young University, Provo, USA

We have investigated the pitch angle (ψ) of the spiral arms of galaxies in the Hubble Space Telescope COSMOS field. The sample consists of 102 face-on galaxies with a two-armed pattern at a mean redshift $\langle z \rangle \approx 0.5$. The typical values of ψ in the spiral arms of distant galaxies are shown to be close to those for nearby spiral galaxies. Within one galaxy the scatter of ψ for different arms is, on average, half the mean pitch angle. In the z range from 1 to 0 we have found a tendency for ψ to decrease. Our analysis of the ψ distributions in galaxies at different redshifts is consistent with the assumption that in most of the galaxies at $z \leq 0.5$ the spiral arms are tidal in origin or they arose from transient recurrent instabilities in their disks.

Keywords: galaxies, photometry, evolution

1. Introduction

Spiral arms are the most prominent feature in most of the bright galaxies in the surrounding part of the Universe. For example, in the local Universe the fraction of such galaxies is $\sim 75\%$ of all the galaxies brighter than an absolute magnitude of -20^m in the B passband (Conselice 2006). A huge number of papers are devoted to investigating the spiral pattern of galaxies (for a recent review, see Sellwood and Masters 2022), but many of the questions related to the formation and maintenance of the existence of spiral arms as well as to their observational manifestations remain poorly studied. The importance of studying these questions stems from the significant influence that the spiral pattern exerts on global processes in a galaxy, for example, on the angular momentum redistribution in the disk (Sellwood and Binney 2002), its stability (Inoue et al. 2021), the star formation rate (Querejeta et al. 2021), the chemical evolution (Scarano and Lépine 2013), etc.

The studies of the spiral pattern of distant galaxies are so far few. It is well known that the familiar types of spiral structure in the nearby Universe

(grand-design, flocculent, multiple arms) were already present at $z \geq 1$ (Elmegreen and Elmegreen 2014). The number density of spiral galaxies drops with increasing z (between $z=0.5$ and $z=2.5$ it decreases approximately by an order of magnitude – Margalef-Bentabol et al. 2022), but objects with a grand-design spiral pattern are encountered even at $z \approx 3$ (Wu et al. 2023).

The main goal of our paper is to investigate the pitch angles in a hundred two-armed spiral galaxies up to a redshift $z \sim 1$.

All of the numerical values in the paper are given for the cosmological model with $\Omega_m = 0.3$, $\Omega_\Lambda = 0.7$, $H_0 = 70 \text{ km s}^{-1} \text{ Mpc}^{-1}$.

2. Sample of galaxies

To study the structure of distant spiral galaxies, we examined the Hubble Space Telescope (HST) COSMOS field (Koekemoer et al. 2007). This field with an area of almost 2 deg^2 was imaged in the F814W filter with ACS. For the selection of objects in COSMOS we used the sample of 26113 bright ($F814W < 22^m$) galaxies in this field presented in

Mandelbaum et al. (2012). For all of the objects from the sample we determined the apparent flattening (b/a) using the SExtractor package (Bertin and Arnouts 1996) and selected 7441 galaxies with $b/a \geq 0.7$. Next, we performed a visual examination of the galaxy images and produced a sample of 184 nearly face-on spiral galaxies with clearly distinguishable spiral arms. During our subsequent analysis we left 102 galaxies with a distinct two-armed spiral pattern in the final sample. We carried out our further analysis of the spiral arms of galaxies (see the next section of the paper) based on the galaxy images reduced to a scale of $0.''03/\text{pixel}$ presented in Mandelbaum et al. (2012).

The sample galaxies were identified with the COSMOS2020 catalog (Weaver et al. 2022). For each object from COSMOS2020 we took the photometric redshifts (their accuracy is $\sim 1\%$) found with the LePhare code (Ilbert et al. 2006), the absolute magnitudes in the r band (Subaru HSC), and the stellar mass estimates in solar masses (M_\odot). Figures 1a and 1b show the positions of the galaxies on the absolute magnitude (M_r) – redshift (z) and galactic stellar mass – z planes. It can be seen from the figures that our sample includes galaxies up to $z \approx 1$ (the mean redshift of the sample is $\langle z \rangle = 0.47 \pm 0.23$), with the galaxies being, on average, bright, $\langle M_r \rangle = -21^m85 \pm 0^m88$, and massive, $\langle \log M_* \rangle = 10.52 \pm 0.43$. Observational selection is also clearly seen in Figs. 1a and 1b: the luminosity and mass of the objects included in the sample increase with z . If we restrict ourselves only to the most massive galaxies with $\log M_* \geq 10.5$ ($M_* \geq 3 \times 10^{10} M_\odot$), then such objects are identified in the entire z range, and the corresponding subsample is relatively complete.

As noted above, galaxies with $b/a \geq 0.7$, which were visually estimated to be oriented nearly face-on, were included in the sample. The mean apparent flattening of the objects in the final sample turned out to be $b/a = 0.87 \pm 0.065$. In our further analysis we did not apply the correction for the possible inclination of the disk plane and assumed the galaxies to be seen exactly face-on.

3. Determination of spiral arms parameters

The procedure of measuring the spiral pattern characteristics is similar to the technique from Savchenko et al. (2020) and is briefly described below. For each galaxy we mark out the individual spiral arms start-

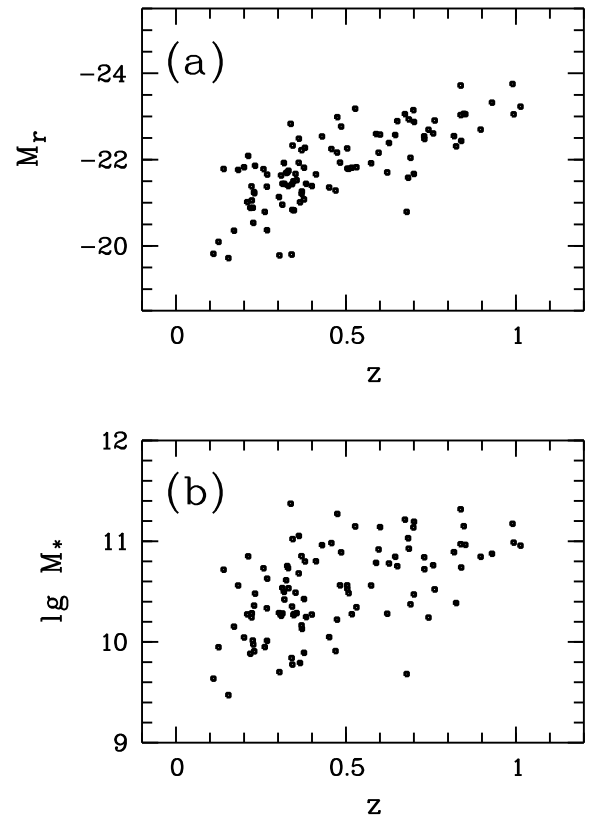


Fig. 1. Redshift dependence of the absolute magnitude of spiral galaxies in the r band (a) and their stellar mass (b).

ing from the bar ends or the central regions and up to the outer regions, where the spiral is still visible above the background level. All of the spirals must be clearly distinguishable and must not contain any branching and self-intersections. Then, based on a special algorithm, at each point of the arm we construct a cut perpendicular to the direction of the spiral and stretched between the minima of the interarm space. Each cut is fitted by an analytically asymmetric Gaussian function in the form

$$I(r) = I_0 \times \exp\left[-\frac{(r - r_{peak})^2}{W_1^2 \cdot s + W_2^2 \cdot (1 - s)}\right],$$

where I_0 denotes the central flux, $W_{1,2}$ are the inner and outer half-widths, r is the distance along the cut, r_{peak} denotes the position of the brightness peak, and the parameter s is equal to 0 if $r \leq r_{peak}$, otherwise 1 (see Fig. 5 in Savchenko et al. 2020). The resulting profile is convolved with the corresponding PSF F814W profile to take into account the influence of the optical system on the images.

Once the fitting has been performed for all of the cuts, we have a completely measured arm model. Examples of the resulting marking after our fitting for four galaxies are shown in Fig. 2. The positions of the peaks r_{peak} are marked by the dots, while the segment size corresponds to the derived half-widths.

The pitch angle ψ is estimated based on the constructed cuts across the spiral arm. For this purpose, the positions of the peaks along the spiral are plotted on the $\log r \div \varphi$ plane, where φ is the polar angle, and then the linear regression is found. The slope of the linear dependence is equal to the sought-for pitch angle ψ , while the root-mean-square (rms) deviation from the straight line gives an estimate of the error in the pitch angle σ_ψ . As a result, in 99 galaxies from the sample we found the pitch angles for both spiral arms; in three galaxies we managed to perform our measurements only for one of the arms.

4. Results and discussion

4.1. Pitch angles

Figure 3 shows the distribution of pitch angles averaged over two arms for 99 sample galaxies that have measurements for both arms. For comparison, the distribution for 31 galaxies from three HST deep fields (HDF-N, HDF-S, HUDF) from Savchenko and Reshetnikov (2011) is shown in the same figure. The galaxies from Savchenko and Reshetnikov (2011) are, on average, at a mean redshift $\langle z \rangle = 0.69 \pm 0.30$, and their pitch angles found based on a Fourier analysis of images were measured in the F606W filter. As can be seen from Fig. 3, the distributions for the two samples of distant galaxies, in which the pitch angles were determined by different methods, agree well. For example, the mean pitch angle for the two-armed spiral galaxies from the COSMOS field is $\langle \psi \rangle = 14.^{\circ}85 \pm 5.^{\circ}51$, while for the galaxies from Savchenko and Reshetnikov (2011) $\langle \psi \rangle = 14.^{\circ}1 \pm 3.^{\circ}5$. If all of the measured arms in COSMOS are considered separately, then the mean value for them is $\langle \psi \rangle = 15.^{\circ}02 \pm 7.^{\circ}05$ (201 spiral arms).

Let us compare the above mean values of ψ with the data for nearby galaxies. For example, $\langle \psi \rangle = 15.^{\circ}2 \pm 3.^{\circ}7$ (50 grand-design galaxies, the g band; Savchenko and Reshetnikov 2013), $\langle \psi \rangle = 18.^{\circ}3 \pm 7.^{\circ}5$ (79 galaxies, the r band; Yu and Ho 2019), $\langle \psi \rangle = 14.^{\circ}8 \pm 5.^{\circ}3$ (155 galaxies, the r band; Savchenko et al. 2020).

In 75 nearby grand-design spiral galaxies from Diaz-

Garcia et al. (2019) the pitch angle shows a dependence on morphological type, i.e., it changes from $13.^{\circ}6 \pm 1.^{\circ}6$ (S0/a–Sab) to $19.^{\circ}7 \pm 2.^{\circ}5$ (Scd–Sdm) (the measurements were made at a wavelength of 3.6 μm). A similar dependence on morphological type is also traceable in other papers (see, e.g., Savchenko et al. 2020). In a large sample of objects (4378 galaxies, the r band; Yu and Ho 2020) the pitch angle varies from $\sim 10^{\circ}$ for Sa-type galaxies to $\sim 30^{\circ}$ for Sd (see Fig. 10 in Yu and Ho 2020).

Thus, the typical pitch angles in galaxies at $z \sim 0.5 - 1$ are close to those for galaxies in the surrounding part of the Universe.

4.2. Scatter of pitch angles

Within one galaxy the spiral arms shows a fairly large scatter of pitch angles. The mean difference in ψ for two spiral arms of the objects from our sample is $\Delta\psi = |\psi_1 - \psi_2| = 6.^{\circ}3 \pm 5.^{\circ}3$. The mean relative variation of the pitch angle is $\Delta\psi/\langle\psi\rangle = 0.48 \pm 0.41$. Thus, the typical scatter of ψ for different arms within one galaxy reaches half the mean pitch angle. The radial ψ variations within the same arm can reach comparable values (Savchenko et al. 2020).

Figure 4 shows the redshift dependence of the error in the pitch angle (σ_ψ) for all of the measured spiral arms. The scatter of data points in the figure is very large, but a certain tendency for σ_ψ to increase with z is traceable. This can imply both the influence of observational selection (the difficulty of measurements in more distant galaxies) and a greater irregularity, clumpiness of the arms in distant galaxies (Elmegreen et al. 2007).

4.3. Evolution of the pitch angle?

The change in the mean pitch angles of the spiral arms of galaxies with redshift is shown in Figs. 5a and 5b. Despite the large scatter of observational data points, a weak trend of ψ with z is noticeable in Fig. 5a. If, alternatively, we consider a subsample of massive spiral galaxies with $\log M_* \geq 10.5$ less distorted by observational selection (Fig. 5b), then this trend becomes more pronounced: from $z = 1$ to $z = 0$ the observed pitch angles decrease, i.e., the spiral arms become, on average, more tightly wound. (The statistical correlation between ψ and z in Fig. 5b is moderate (its Spearman rank correlation coefficient is 0.38), but significant at $>99\%$.) The linear depen-

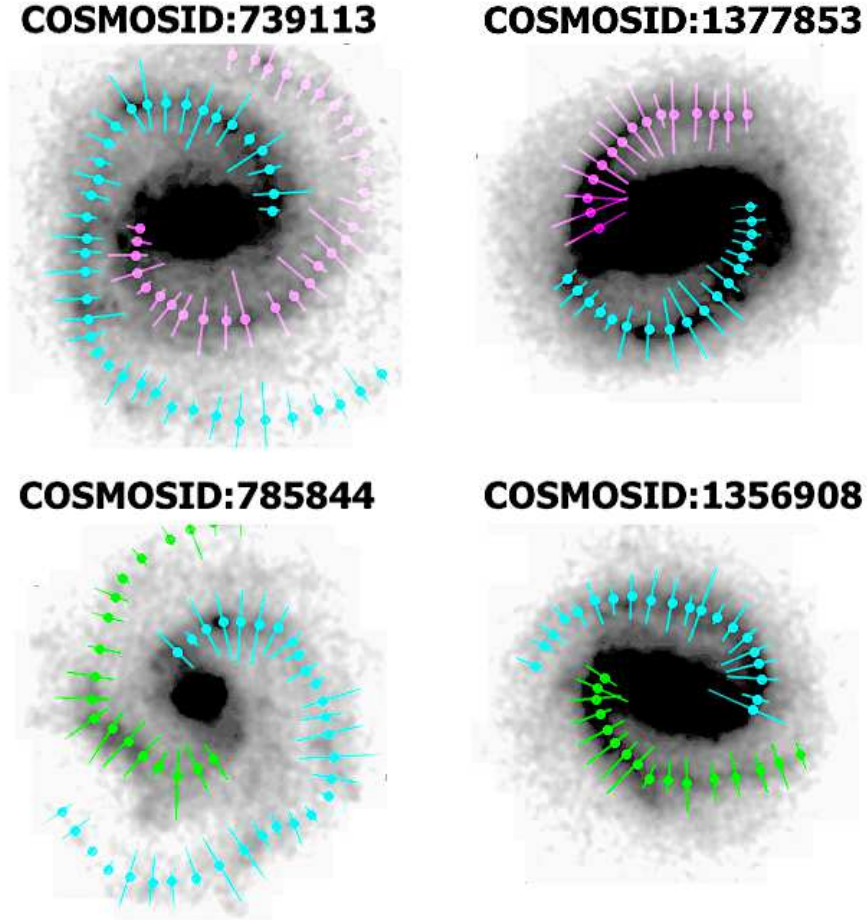


Fig. 2. Examples of galaxies from the sample with measured spirals. The dots mark the positions of the brightness peaks; the segments correspond to the spiral half-width.

dence shown in Fig. 5b corresponds to a winding rate $\sim 1^\circ/\text{Gyr}$.

A possible reason for the existence of the observed trend between ψ and z can be the influence of the k -correction, i.e., the fact that when passing to more distant galaxies, we see their images in an increasingly short wavelength range. If the arm pitch angle depends on wavelength (λ) in such a way that ψ increases with decreasing λ , then this could explain at least in part Fig. 5. As said above, our measurements were performed in the HST ACS/F814W filter with an effective wavelength $\lambda_{eff} \approx 8000 \text{ \AA}$, i.e., approximately in the I band. When objects at $z = 1$ are observed, this filter will roughly correspond to the B band. A direct comparison of the pitch angles for nearby galaxies found in blue filters (B, g) and in the near infrared showed no significant differences (see, e.g., Seigar et al. 2006; Davis et al. 2012; Savchenko et al. 2020). In addition, there is evidence that the spiral arm pitch angle can decrease when passing from “red” to “blue” filters (Yu and Ho 2018). If this is the case,

then this even enhances the significance of the observational trend in Fig. 5. Yet another reason can be observational selection when selecting objects: among more distant galaxies the probability to miss galaxies with tightly wound spiral arms is higher due to the lower spatial resolution. Both these effects, the influence of the k -correction and observational selection, need a further study.

It is also worth noting that as the spiral galaxies evolve from $z \sim 1$ to $z \sim 0$, the luminosity of the bulges increases and their contribution to the total luminosity of the galaxies grows (see, e.g., Sachdeva et al. 2017). On the other hand, it was noted in a number of papers that in galaxies with brighter bulges and a higher concentration of the luminosity to the center the values of ψ are, on average, lower than those in galaxies with fainter bulges and a lower concentration (see, e.g., Savchenko and Reshetnikov 2013; Yu and Ho 2020). Thus, the change in the pitch angle with z can at least in part be a consequence of the evolution of the global structure of galaxies.

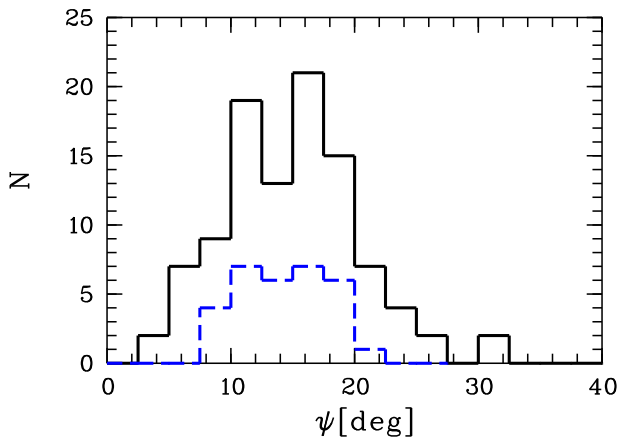


Fig. 3. Distribution of galaxies from the COSMOS field in mean pitch angle (solid line); the corresponding distribution for galaxies from three HST deep fields is indicated by the blue dashed line (Savchenko and Reshetnikov 2011).

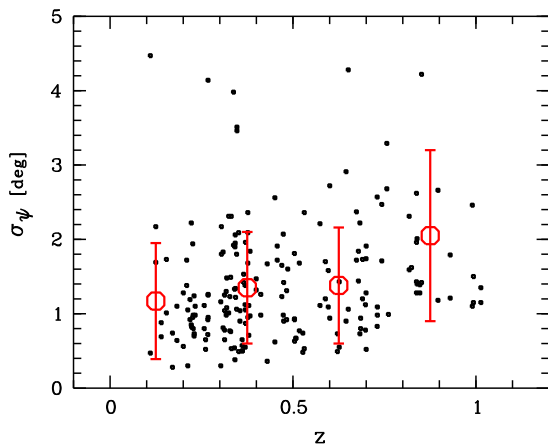


Fig. 4. Redshift dependence of the rms deviation of the spiral arm pitch angle. The circles with bars are the mean values in z bins 0-0.25, 0.25-0.5, 0.5-0.75, and 0.75-1.0.

Different spiral structure generation and maintenance models predict a different behavior of the pitch angle as a function of time. For example, in the models in which the arms arise from a tidal perturbation and/or transient spiral instabilities in a self-gravitating disk, the angle ψ can decrease with time (for a review, see Dobbs and Baba 2014). At the same time, in the density wave theory (Lin and Shu 1964) the spiral pattern is quasi-stationary with an invariable pitch angle.

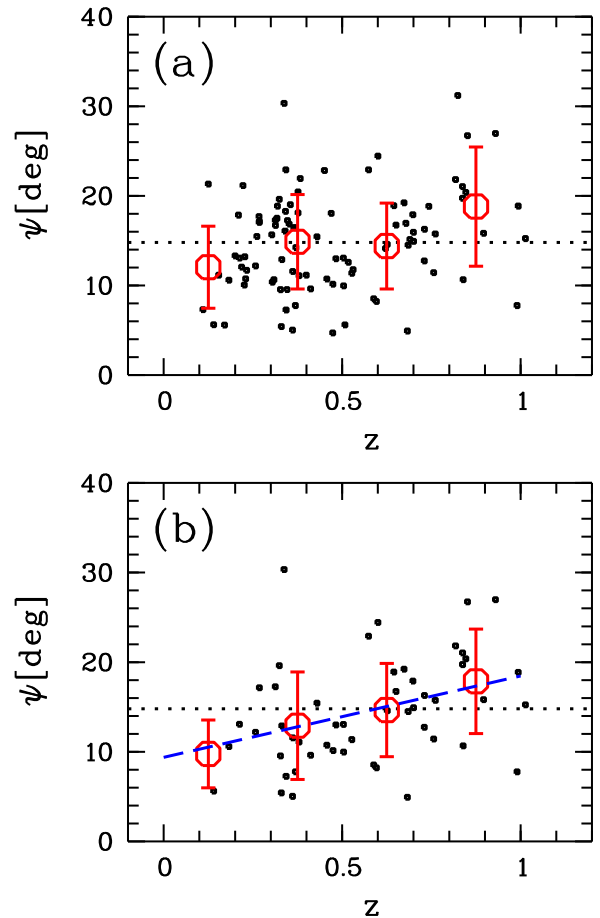


Fig. 5. Redshift dependence of the mean spiral pattern pitch angle: (a) the entire sample and (b) the galaxies with $\log M_* \geq 10.5$. The circles with bars in both figures are the mean values in z bins 0-0.25, 0.25-0.5, 0.5-0.75, and 0.75-1.0. The horizontal dotted lines indicate the mean value of ψ for the entire sample, the dashed line is the linear regression for massive spiral galaxies.

A simple observational test has recently been proposed for transient and recurrent spiral arms (Pringle and Dobbs 2019). Let the spiral arm during its formation have a pitch angle ψ_{max} , the arm then gradually winds up and, finally, disappears at some minimum ψ_{min} . Then, based on simple reasoning, we can find that the cotangent of the pitch angle changes linearly with time: $\cot \psi \propto t$. Consequently, if at an arbitrary instant of time we will consider a random sample of galaxies in which the spiral arms are at different winding stages, then one might expect the galaxies to be distributed uniformly in $\cot \psi$ in the range from $\cot \psi_{min}$ to $\cot \psi_{max}$. The application of this test for two samples of nearby galaxies, to a first approximation, confirmed the uniformity of the $\cot \psi$

distribution (Pringle and Dobbs 2019; Lingard et al. 2021).

Let us consider how the distant galaxies in the COSMOS field are distributed in $ctg\psi$. We took a relatively complete subsample of galaxies with $\log M_* \geq 10.5$, for which there are ψ measurements for 85 individual spiral arms. Figures 6 and 7 present the distributions of galaxies in ψ and $ctg\psi$ in four z bins. (The bins were chosen in such a way that approximately the same number of galaxies fell into them.) To a first approximation, the distributions shown in Fig. 6 are nonuniform, and their means are shifted toward smaller ψ with decreasing redshift. When passing to $ctg\psi$, the shape of the distributions changes (Fig. 7): in the first two redshift bins the distributions are nearly uniform (of course, within the limits of poor statistics), in agreement with the results of recent works in which nearby galaxies were studied (Pringle and Dobbs 2019; Lingard et al. 2021). At $z > 0.5$ the distributions exhibit global peaks at $ctg\psi \approx 3$ ($\psi \approx 18^\circ$). The change in the shape of the distributions with redshift can imply that different spiral pattern generation mechanisms could prevail at different epochs.

5. Conclusions

In our paper for the first time we have considered in detail the shape of the spiral arms in two-armed galaxies in the HST COSMOS field.

We found that the typical values of the spiral pattern pitch angle up to $z \sim 1$, $\langle\psi\rangle \approx 15^\circ$, are close to those for nearby galaxies.

Within one galaxy different spiral arms exhibit greatly differing pitch angles. For individual arms the error in ψ increases with z , which may be a consequence of their growing irregularity.

We found an observational trend suggesting a gradual decrease in ψ with decreasing z (Fig. 5). This trend corresponds to a mean winding rate $\sim 1^\circ/\text{Gyr}$.

Our analysis of the $ctg\psi$ distributions (the Pringle-Dobbs test) in massive galaxies ($\log M_* \geq 10.5$) for different redshift bins is consistent with the fact that at $z \leq 0.5$ tidal perturbations and transient instabilities in their disks could be the main spiral arm generation mechanisms. Applying this test for large samples of spiral galaxies at different redshifts can become a useful tool for studying the evolution of the spiral pattern.

Note that our results are based on a relatively small sample of objects, and they need to be confirmed on

much more extensive material. A combination of the data from HST and JWST deep fields with the development of computer image analysis methods will soon make it possible to investigate the questions touched on in our paper in much more detail.

6. Funding

This work was supported by the Russian Science Foundation (project no. 22-22-00483).

References

- E. Bertin and S. Arnouts, *Astron. Astrophys. Suppl. Ser.* 117, 393 (1996).
- C.J. Conselice, *Mon. Not. R. Astron. Soc.* 373, 1389 (2006).
- B.L. Davis, J.C. Berrier, D.W. Shields, et al., *Astrophys. J. Suppl. Ser.* 199, 33 (2012).
- S. Diaz-Garcia, H. Salo, J. H. Knapen, and M. Herrera-Endoqui, *Astron. Astrophys.* 631, A94 (2019).
- C. Dobbs and J. Baba, *Publ. Astron. Soc. Austr.* 31, e035 (2014).
- D.M. Elmegreen, B.G. Elmegreen, T. Ferguson, and B. Mullan, *Astrophys. J.* 663, 734 (2007).
- D.M. Elmegreen and B.G. Elmegreen, *Astrophys. J.* 781, 11 (2014).
- O. Ilbert, S. Arnouts, H. J. McCracken, et al., *Astron. Astrophys.* 457, 841 (2006).
- S. Inoue, T. Takagi, A. Miyazaki, et al., *Mon. Not. R. Astron. Soc.* 506, 84 (2021).
- A.M. Koekemoer, H. Aussel, D. Calzetti, et al., *Astrophys. J. Suppl. Ser.* 172, 196 (2007).
- C.C. Lin and F.H. Shu, *Astrophys. J.* 140, 646 (1964).
- T. Lingard, K.L. Masters, C. Krawczyk, et al., *Mon. Not. R. Astron. Soc.* 504, 3364 (2021).
- R. Mandelbaum, Ch.M. Hirata, A. Leauthaud, R.J. Massey, and J. Rhodes, *Mon. Not. R. Astron. Soc.* 420, 1518 (2012).
- B. Margalef-Bentabol, Ch.J. Conselice, B. Haeussler, et al., *Mon. Not. R. Astron. Soc.* 511, 1502 (2022).

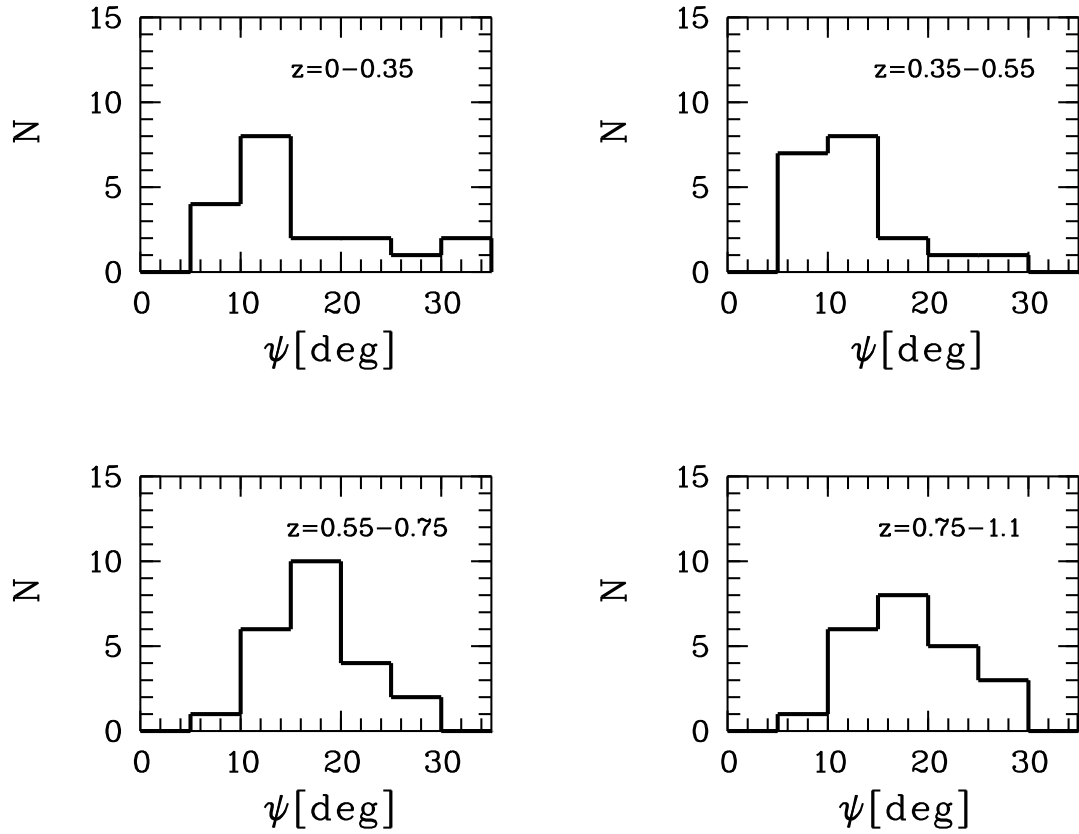


Fig. 6. Distributions of spiral arm pitch angles ψ for the massive galaxies from the sample ($\log M_* \geq 10.5$) in different redshift bins.

J.E. Pringle and C.L. Dobbs, Mon. Not. R. Astron. Soc. 490, 1470 (2019).

M. Querejeta, E. Schinnerer, S. Meidt, J. Sun, A.K. Leroy, et al., Astron. Astrophys. 656, A133 (2021).

S. Sachdeva, K. Saha, and H.P. Singh, Astrophys. J. 840, 79 (2017).

S.S. Savchenko and V.P. Reshetnikov, Astron. Lett. 37, 817 (2011).

S.S. Savchenko and V.P. Reshetnikov, Mon. Not. R. Astron. Soc. 436, 1074 (2013).

S. Savchenko, A. Marchuk, A. Mosenkov, and K. Grishunin, Mon. Not. R. Astron. Soc. 493, 390 (2020).

S. Scarano and J. R. D. Lépine, Mon. Not. R. Astron. Soc. 428, 625 (2013).

M.S. Seigar, J.S. Bullock, A.J. Barth, and L.C. Ho, Astrophys. J. 645, 1012 (2006).

J.A. Sellwood and K.L. Masters, Ann. Rev. Astron. Astrophys. 60, 73 (2022).

J.A. Sellwood and J.J. Binney, Mon. Not. R. Astron. Soc. 336, 785 (2002).

J.R. Weaver, O.B. Kauffmann, O. Ilbert, et al., Astrophys. J. Suppl. Ser. 258, 11 (2022).

Y. Wu, Z. Cai, F. Sun, et al., Astrophys. J. Lett. 942, id.L1 (2023).

S.-Yu. Yu and L.C. Ho, Astrophys. J. 869, 29 (2018).

S.-Yu. Yu and L.C. Ho, Astrophys. J. 871, 194 (2019).

S.-Yu. Yu and L.C. Ho, Astrophys. J. 900, 150 (2020).

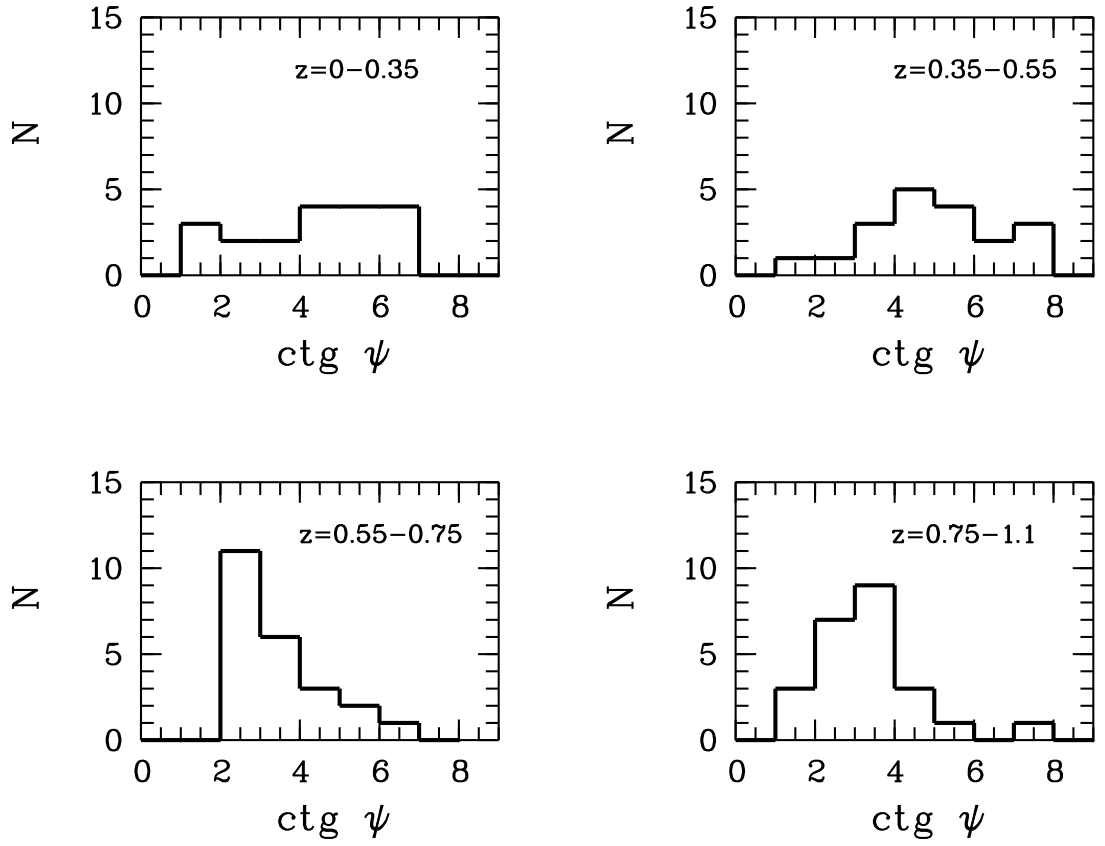


Fig. 7. Distributions of $ctg \psi$ for the spiral arms of the massive galaxies from the sample ($\log M_* \geq 10.5$) in different redshift bins.